Comparison of three models for winter wheat yield prediction based on UAV hyperspectral images

Xiaobin Xu[1], Cong Teng[1,2], Hongchun Zhu[1], Haikuan Feng[2], Yu Zhao[2], Zhenhai Li[1*]

(1. *College of Geodesy and Geomatics, Shandong University of Science and Technology, Qingdao 266590, Shandong, China*;
2. *Key Laboratory of Quantitative Remote Sensing in Ministry of Agriculture and Rural Affairs, Information Technology Research Center, Beijing Academy of Agriculture and Forestry Sciences, Beijing 100097, China*)

Abstract: Predicting crop yield timely can considerably accelerate agricultural production management and food policy-making, which are also important requirements for precise agricultural development. Given the development of hyperspectral imaging technology, a simple and efficient modeling method is convenient for predicting crop yield by using airborne hyperspectral images. In this study, the Unmanned Aerial Vehicle (UAV) hyperspectral and maturity yield data in 2014-2015 and 2017-2018 were collected. The winter wheat yield prediction model was established by optimizing Vegetation Indices (VIs) feature scales and sample scales, incorporating Partial Least Squares Regression (PLSR), Random Forest algorithm (RF), and Back Propagation Neural Network algorithm (BPN). Results showed that PLSR stands out as the optimal wheat yield prediction model considering stability and accuracy (RMSE=948.88 kg/hm^2). Contrary to the belief that more input features result in higher accuracy, PLSR, RF, and BPN models performed best when trained with the top 3, 8, and 4 VIs with the highest correlation, respectively. With an increase in training samples, model accuracy improves, reaching stability when the training samples reach 70. Using PLSR and optimal feature scales, UAV yield prediction maps were generated, holding significant value for field management in precision agriculture.

Keywords: hyperspectral imagery, unmanned aerial vehicle, winter wheat, yield prediction model, remote sensing
DOI: 10.25165/j.ijabe.20241702.5869

Citation: Xu X B, Teng C, Zhu H C, Feng H K, Zhao Y, Li Z H. Comparison of three models for winter wheat yield prediction based on UAV hyperspectral images. Int J Agric & Biol Eng, 2024; 17(2): 260–267.

1 Introduction

Food shortage has been a global concern, which is related not only to the national economy and people's livelihood but also to the essence of national development[1]. Winter wheat is one of the primary grain crops, and the accurate and timely prediction of wheat yield information has been the focus of studies on agriculture[2]. Currently, research on predicting crop yields primarily revolves around traditional sample estimation and Remote Sensing (RS)[3]. While traditional methods offer high precision, they necessitate substantial human resources and equipment costs[4]. In contrast, hyperspectral RS technology is distinguished by its high spectral resolution, strong band continuity, and abundant spectral information[5]. This technology provides an opportunity for monitoring crop growth and predicting yields in a timely, efficient, and non-invasive manner[6,7].

In the field of precision agriculture, RS yield prediction devices are mainly categorized into proximal handheld devices[8] and Unmanned Aerial Vehicle (UAV) platforms[9]. While proximal handheld devices can achieve non-destructive advance yield predictions, they still exhibit significant gaps in terms of timeliness and regional coverage when compared to UAV platforms[10]. UAV platforms, equipped with sensors, offer a flexible, rapid, and non-invasive means for conducting multi-temporal observations of field wheat, leading to the generation of yield prediction maps[11]. These platforms can be outfitted with various sensors, such as RGB, multispectral, and hyperspectral cameras, enabling the capture of diverse data for comprehensive analysis. RGB and multispectral cameras, due to their low cost and portability, have become the most commonly used tools currently[12-14]. However, their limited spectral resolution restricts their potential applications in quantitative agriculture. High spectral resolution narrowband cameras can capture richer spectral information and finer surface features, offering enhanced practical value in various applications[15,16]. Fan et al.[17] successfully estimated corn yield using the full-band reflectance obtained from a UAV-mounted hyperspectral camera. Utilizing high-resolution UAV hyperspectral reflectance data, Kaes et al.[18] estimated wheat LAI (leaf area index) and chlorophyll, subsequently employing this information for yield prediction. However, hyperspectral data often involve hundreds of bands, posing challenges such as large data volume, information redundancy, and complexity in band selection for yield estimation based on full-spectrum reflectance[19]. In contrast, Vegetation Indices (VIs), typically derived from a few selected bands, offer a more straightforward and intuitive expression of vegetation status and growth conditions[20,21]. They have been widely employed in RS crop yield estimation[22,23]. In recent years, the increasing number of VIs associated with crop growth and yield information has posed a new challenge in determining which and how many VIs should be selected as optimal features for crop yield prediction models.

Received date: 2020-05-11 **Accepted date:** 2021-05-18
Biographies: Xiaobin Xu, PhD candidate, research interest: agricultural remote sensing, Email: xuxb77@whu.edu.cn; **Cong Teng**, MS, research interest: agricultural remote sensing, Email: 862696556@qq.com; **Hongchun Zhu**, PhD, professor, research interest: remote sensing and GIS applications, Email: sdny_xa@163.com; **Haikuan Feng**, PhD candidate, research interest: agricultural remote sensing, Email: fenghaikuan123@163.com; **Yu Zhao**, PhD, research interest: agricultural remote sensing, Email: zy928286257@163.com.
***Corresponding author: Zhenhai Li**, PhD, professor, research interest: agricultural remote sensing. College of Geodesy and Geomatics, Shandong University of Science and Technology, Qingdao 266590, Shandong, China. Email: lizh323@126.com.

As computer capabilities for data processing and analysis continue to advance, a multitude of RS yield prediction models based on statistical regression and machine learning have emerged[24-26]. Tan used the Partial Least Squares Regression (PLSR) algorithm to analyze the quantitative relationship between satellite RS variables and actual wheat yield and reported that the PLSR algorithm is better than the linear regression and principal component analysis algorithm[27]. Su et al.[28] showed that Back Propagation Neural Network (BPN) could be better applied for grain yield prediction than methods by stepwise regression and gray correlation modeling. Yue et al.[29] utilized a Random Forest (RF) algorithm to combine spectral data with VIs for the regression modeling of winter wheat biomass and confirmed the potential of the RF algorithm for the RS prediction of winter wheat biomass. However, in most studies utilizing these algorithms for crop yield prediction, various VIs were directly used as input features without pre-optimization of these features[30,31]. Furthermore, randomness is a characteristic of these models, and differences in model randomness and initial conditions often yield stochastic results, leading to insufficient stability in crop yield prediction[32,33]. Therefore, it is crucial to further investigate how the stability in the output results of these yield prediction models is influenced by the size of features and samples.

In addressing the aforementioned issues, this study utilized high-spectral data from 2014-2015 and 2017-2018 to compute and screen multiple VIs. Using the PLSR, BPN, and RF algorithms, wheat yield prediction models were constructed based on different feature and sample scales. The objectives were as follows: 1) to select the optimal yield prediction model; 2) to determine the optimal number of features for different yield prediction models; 3) to assess the impact of varying sample sizes on the stability and accuracy of the yield prediction models.

2 Materials and methods

2.1 Study area and experimental design

The experimental design was performed during the growing seasons of 2014-2015 and 2017-2018 at the Xiaotangshan experimental site (116.44°E, 40.18°N) in Beijing, China (Figure 1). The experimental site is located at an average altitude of 36 m and has a warm temperate semi-humid continental monsoon climate. This climate is mild and has four distinct seasons. Experiment (Exp.) 1 was designed as three-way factors of cultivar, nitrogen, and irrigation treatments during the growing season of 2014-2015. The winter wheat cultivars were Jing9843 (J9843) and Zhongmai175 (ZM175). The nitrogen fertilizer treatments were 0, 195, 390, and 585 kg/hm^2, respectively. Irrigation was designed as rainfall (0 mm), normal irrigation (192 mm), and excess irrigation (384 mm). A total of 48 experiment plots with 16 treatments and three replicates is shown in Figure 1. Exp. 2 included two experimental designs, one was designed as completely randomized two-way factorial combinations of two cultivars (Lunxuan167 and Jingong18) and four nitrogen fertilizer rates, the same as Exp. 1, during the growing season of 2017-2018 (Figure 1). The other was designed as completely randomized two-way factorial combinations of two cultivars (Lunxuan167 and Jingdong18) and four nitrogen-recommended fertilizer rates (Table 1).

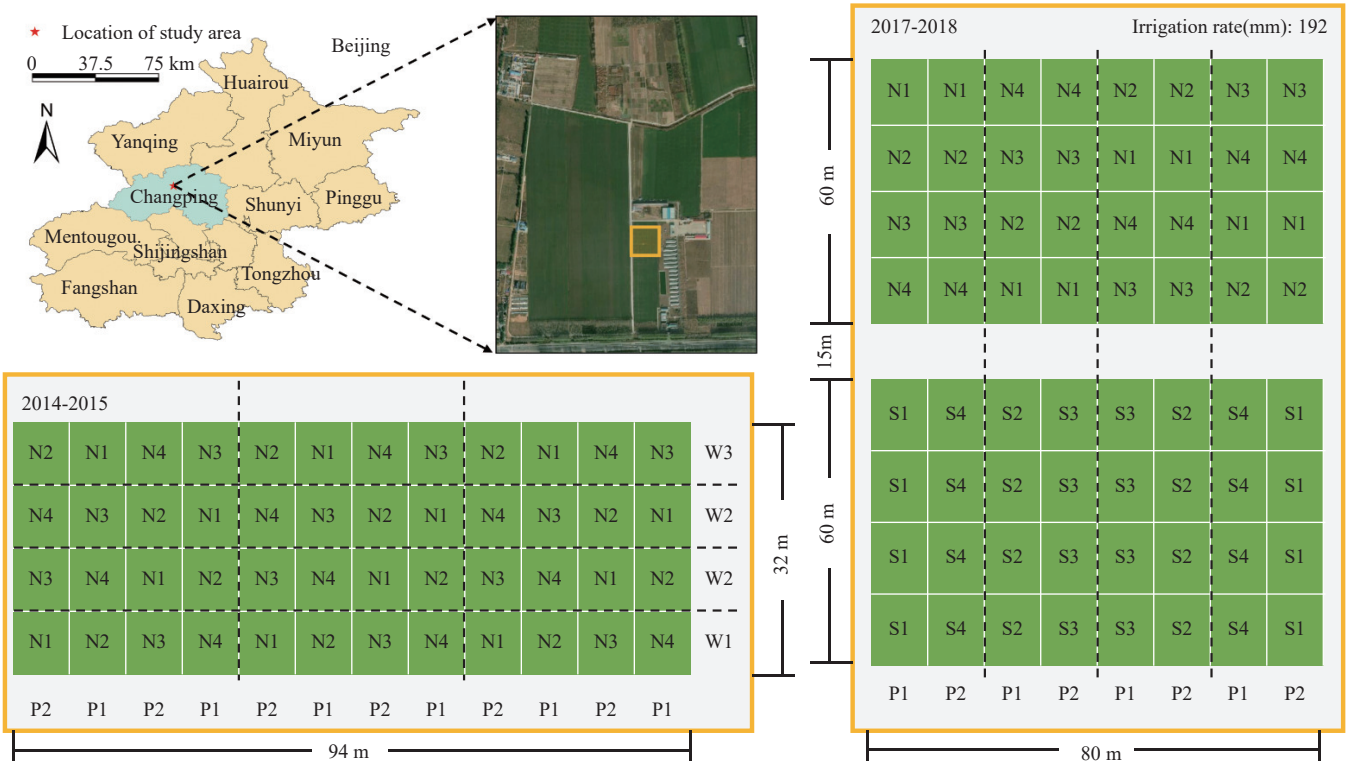

Note:
Cultivar: Jing9843 (P1); Zhongmai175 (P2) Irrigation rate (mm): Rainwater (W1); 192 (W2); 384 (W3)
Nfertilizerrate (kg/ha): 0 (N1); 195 (N2); 390 (N3); 585 (N4)

Figure 1 Overview of the experiment area and distribution of experiment plots

2.2 Data acquisition

2.2.1 UAV Hyperspectral data acquisition

The UAV hyperspectral images were acquired during the flowering stage of wheat on May 13, 2015, and May 14, 2018. In this experiment, an eight-rotor UAV was used as a platform to carry a UHD185 imaging spectrometer (Cubert, Germany) with a

Table 1 Recommended nitrogen fertilizer (kg/hm²) applied during the growing season of 2017-2018

Treatments	Fertilizing date		Treatments	Fertilizing date	
	8th April	4th May		8th April	4th May
S01	78	0	S17	112	0
S02	0	0	S18	110	130
S03	0	10	S19	0	28
S04	78	0	S20	180	0
S05	34	25	S21	30	52
S06	0	0	S22	0	203
S07	38	82	S23	23	97
S08	140	0	S24	154	0
S09	142	0	S25	148	0
S10	30	0	S26	50	175
S11	0	145	S27	0	464
S12	100	0	S28	178	0
S13	33	7	S29	30	111
S14	0	21	S30	0	114
S15	124	21	S31	132	148
S16	27	0	S32	93	0

Note: base fertilizer nitrogen rates were 195 kg/hm² for all treatments.

spectrum ranging from 450 nm to 950 nm (Figure 2). The UAV flew at a constant speed of 5 m/s at an altitude of 50 m above the plot, capturing hyperspectral images with a spatial resolution of 21 cm. The winter wheat field was photographed from 10:00 to 14:00 Beijing time when it was sunny day and cloudless. The original images of the UAV-included radiation correction and atmospheric correction were subjected to data processing by using ENVI (Exelis Visual Information Solutions, USA)[34], image fusion by using Cubert Pilot (Cubert, Germany), and hyperspectral image mosaic by using Agisoft PhotoScan (Agisoft LLC, Russia) to eliminate the influence of atmospheric transmission and sensors in the imaging process and to integrate hyperspectral and high-spatial-resolution images. The spectral curve of the experimental area was extracted and studied using ArcGIS (Esri, USA). Detailed process flow is shown in Figure 3.

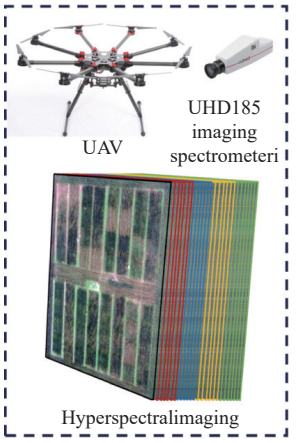

Technical properties of UHD 185	
Wavelength range	450-950 nm
Sampling interval	4 nm
Spectral resolution	8 nm@532 nm
Channels	125
Detector	Si CCD
Weight	470 g
Housing	28 cm×6.5 cm×7 cm
Digitization	12 bit
Field angle	19°
Cube resolution	1 megapixel
Spectral throughput	2500 spectra/cube
Power	DC 12 V, 15 W

Figure 2 Unmanned aerial vehicle (UAV), UHD185 hyperspectral imaging spectrometer, and its technical parameters

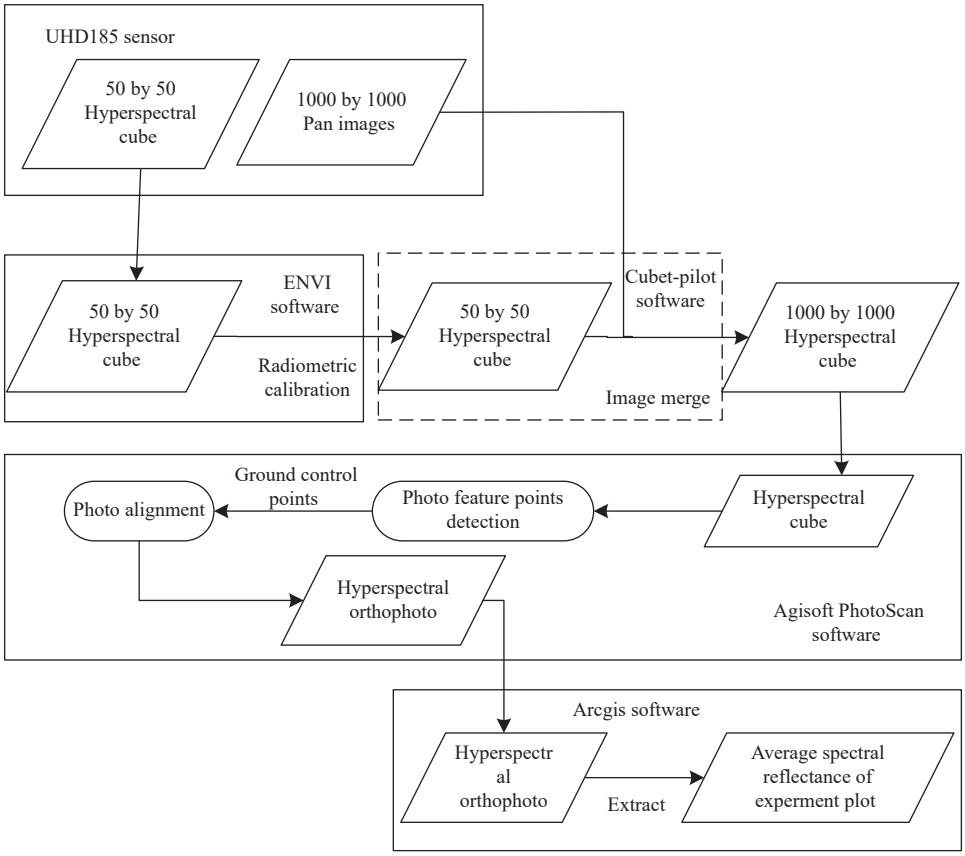

Figure 3 Preprocessing of UAV remote sensing data

2.2.2 Yield data

The yield data were collected during the maturity of winter wheat. Yield data were collected at the maturation stage of winter wheat, which was randomly selected from the sample in the experimental area. Then, the collected samples were threshed, dried, and weighed (the accuracy of the electronic balance was 0.01 g). A total of 112 samples were randomly divided into two sets: 90 samples for the modeling set and 22 samples for the validation set.

Throughout the experiment, the yield ranged from 800 to 8998 kg/hm^2, with the modeling set encompassing a production data range of 800-8998 kg/hm^2 and the validation set having a yield data range of 1895-8899 kg/hm^2. The average yield value in the modeling set was 5719 kg/hm^2, which closely matched the average value in the validation set at 5739 kg/hm^2.

2.3 Models and methods

2.3.1 Vegetation index (VI)

Ten commonly used VIs were selected as parameters to predict the yield of winter wheat in accordance with previously described methods. Choose the VI suitable for predicting winter wheat yield by using the UAV. The mathematical formula is listed in Table 2.

Table 2 Summary of vegetation index (VI) in this study

Name	Formula	References
Red-edge Chlorophyll Index	$CI_{red\ edge} = (R_{750}/R_{720})-1$	Gitelson et al., 2005[35]
Double-peak Canopy Nitrogen Index	$DCNI = (R_{720}-R_{700})/(R_{700}-R_{670})/(R_{720}-R_{670}+0.03)$	Chen et al., 2010[36]
Green Index	$GI = R_{551}/R_{677}$	Zarco-Tejada et al., 2005[37]
Green Normalized Difference Vegetation Index	$GNDVI = (R_{750}-R_{550})/(R_{750}+R_{550})$	Baret et al., 1991[38]
Modified red-edge Simple Ratio Index	$MSR = (R_{800}/R_{670}-1)/sqrt(R_{800}/R_{670}+1)$	Chen 1996[39]
Red Edge Normalized Index	$ND705 = (R_{750}-R_{705})/(R_{750}+R_{705})$	Sims et al., 2002[40]
Normalized Difference Red Edge	$NDRE = (R_{790}-R_{720})/(R_{790}+R_{720})$	Fitzgerald et al., 2010[41]
Normalized Difference Vegetation Index	$NDVI = (R_{890}-R_{670})/(R_{890}+R_{670})$	Bouman et al., 1992[42]
Normalized Difference Vegetation Index canste	$NDVI_{canste} = (R_{760}-R_{708})/(R_{760}+R_{708})$	Steddom et al., 2003[43]
Spectral Polygon Vegetation Index	$SPVI = 0.4(3.7(R_{800}-R_{670})-1.2abs(R_{550}-R_{670}))$	Verrelst et al., 2008[44]

Note: R_{xxx} represents the spectral reflectance at *xxx* nm.

2.3.2 Partial Least Squares Regression (PLSR) model

The PLSR is a multivariate statistical analysis method that integrates the characteristics of multiple linear regression analysis, canonical correlation analysis, and principal component analysis. PLSR is the most common set of data by minimizing the sum of squared errors, which can be modeled under the condition of the serious multi-dependency of independent variables and solve the problem wherein the number of samples is smaller than the number of variables. PLSR can also interpret independent and dependent variables. Therefore, PLSR is widely used for RS to invert biomass parameters[45]. The final model in predicting yield (y) has the following specific form:

$$y = b_0 + b_1 t_1 + b_2 t_2 + ... + b_n t_n \quad (1)$$

where, t_1 to t_n are the numbers of copies of the principal component from 1 to n, and b_n is the regression coefficient. The n of this study is determined by the number of input features, with a range of n between 3 and 8.

2.3.3 Random Forest (RF) model

The RF is a classification tree-based algorithm proposed by Breiman and Cutler in 2001[46]. As shown in Figure 4, RF consists of several decision trees with multiple trees used to simulate training samples. The final classification result is voted by a multitree classifier[47]. RF summarizes a large number of classification trees and improves the prediction accuracy of a model. The RF operation speed is fast and does not need to consider multicollinearity problems. The RF operation also performs well in dealing with big data. RF is a new model that replaces traditional machine learning models, such as neural networks[48].

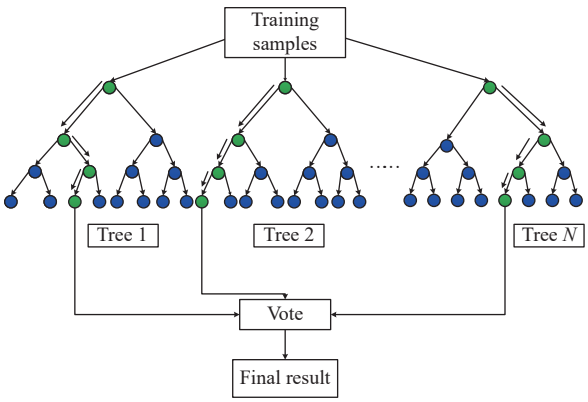

Figure 4 Schematic diagram of random forest (RF) classification process

2.3.4 Back Propagation Neural Network (BPN) model

The BPN is one of the most widely used and most effective neural network models[49]. A BPN prediction model with a single hidden layer is constructed using the trainlm training function and the learngdm adaptive learning function in MATLAB R2016a (MathWorks, USA). Tansig is used as a transfer function for the hidden and output layers. The output calculation results of the BPN model are as follows:

$$Y = f^2(w^2 f^1(w^1 X + b^1) + b^2) \quad (2)$$

where, Y is the output vector (predicted yield); X is the input vector; f^1 and f^2 are the transfer functions on the hidden and output layers, respectively; b^1 and b^2 are the deviations of the hidden and output layers, respectively; w^1 and w^2 are the weights of the layer and hidden layer, respectively[50].

2.4 Statistical analysis

In this study, the performance of the models was evaluated using Root Mean Square Error (RMSE) and Coefficient of Variation (CV). RMSE reflects the degree of deviation between the simulated and measured values. Generally, a lower RMSE indicates higher accuracy in modeling and validation. The RMSE was calculated as follows:

$$RMSE = \sqrt{\frac{1}{n}\sum_{i=1}^{n}(Y_i - Y_i')^2} \quad (3)$$

where, Y_i is the measured value; Y_i' is the predicted value, and n is the number of samples. The CV is a normalized measure of the variability of each statistical value. A smaller CV indicates less variability and higher reliability of the model. Conversely, a larger CV suggests greater variability and lower reliability of the model. The CV was calculated as follows:

$$CV = \frac{SD}{MN} \quad (4)$$

where, SD is the standard deviation, and MN is the average.

3 Results

3.1 Selection of Vegetation index

Table 3 lists the correlation between VIs and winter wheat

yield. All tested VIs showed an extremely significant correlation with yield (p<0.01), with NDRE exhibiting the highest correlation (r=0.792) and GI displaying the lowest correlation (r=0.634). The ranking of VIs in terms of their correlation with yield, from highest to lowest, is NDRE, CIred edge, NDVIcanste, ND705, NDVI, MSR, GNDVI, DCNI, SPVI, and GI. In this study, feature parameters for model construction were selected by choosing the top three to eight VIs in descending order.

Table 3 Correlation coefficient (r) between VI and yield

VI	r	VI	r
$CI_{red\ edge}$	0.779**	ND705	0.758**
DCNI	0.646**	NDRE	0.792**
GI	0.634**	NDVI	0.732**
GNDVI	0.716**	$NDVI_{canste}$	0.767**
MSR	0.717**	SPVI	0.640**

Note: ** indicates that the correlation reached a very significant level (p<0.01).

3.2 Performance of models with varying numbers of input features

Three yield prediction models for winter wheat were constructed based on PLSR, RF, and BPN, respectively. Random sampling was conducted 1000 times for the three models to verify the practicability of the model and the influence of sampling results on the model construction. In the verification set, the predicted values of the three methods were compared with the measured values (Figure 5). Regardless of the number of selected features and multiple runs, the PLSR method demonstrates the strongest stability. When modeling with three VIs, the PLSR method achieves the best prediction performance (RMSE=948.8 kg/hm^2). In contrast, the stability of predictions by the RF method is less satisfactory, with RMSE ranging from 907.93 to 1091.90 kg/hm^2. However, the accuracy of the RF model increases with an increase in the number of VIs, reaching optimal results when using eight indices. The BPN method exhibits the poorest stability in yield prediction, with the most pronounced RMSE fluctuations (841.56-1147.58 kg/hm^2). As the number of VIs increases, the fluctuation of RMSE gradually rises. When using three, eight, and four VIs, PLSR, RF, and BPN models show the highest accuracy (Figure 5). The yield prediction results of the three models with the optimal selected features are illustrated in Figure 6. Although RF demonstrates the highest fitting accuracy in the modeling set, PLSR exhibits lower prediction errors in the more critical validation set. In summary, considering both stability and accuracy, all three methods can be utilized for yield prediction, with PLSR outperforming the BPN and RF models.

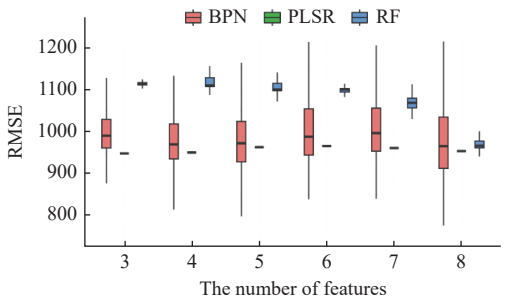

Figure 5 Performance variations of models with different feature sizes

3.3 Performance of models with varying numbers of training samples

To assess the impact of varying training sample sizes on the models, the three models based on optimal feature selection were trained with different randomly selected sample quantities in the training set. The sample size in the validation set remained constant, and the results were evaluated for stability through 1000 repetitions, as depicted in Figure 7 and Table 4. In instances where the sample size was excessively small, such as having only 10 samples, the predictive models based on the three methods exhibited instability (CV_PLSR=0.39, CV_RF=0.16, CV_BPN=4.42). With an increase in sample size, the predictive models for the three methods tended to stabilize, showcasing low RMSE values and small CVs. In scenarios of large sample sizes, the RMSE values of models predicted using the PLSR and RF methods were close, with the PLSR method demonstrating high fitting. However, for sample sizes less than 20, the CV of the model based on the PLSR method was substantial (CV>0.2), indicating lower stability. At a sample size of 90, the RMSE of the predicted model based on the three methods approached 1000 kg/hm^2, but the model based on the BPN method exhibited the worst stability and the lowest fitting effect. Accuracy was significantly influenced by the sample size. Therefore, the yield prediction model constructed based on the PLSR method was applied to UAV hyperspectral imaging in this study.

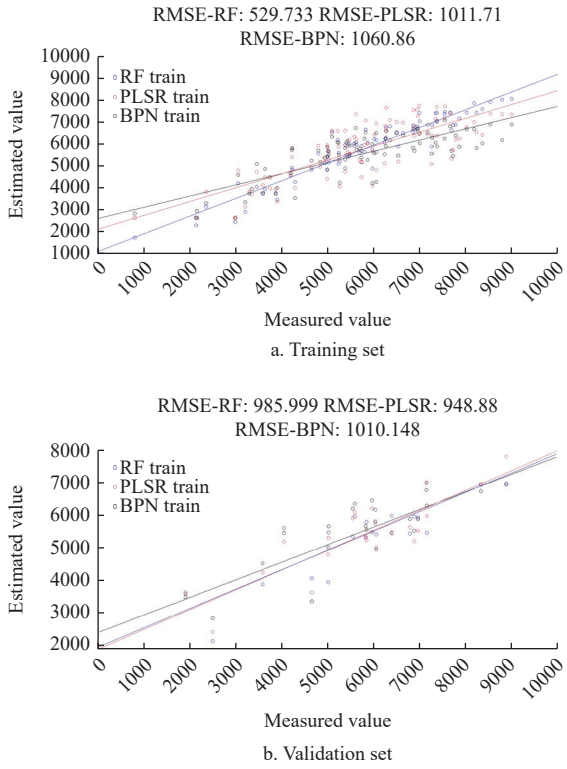

Figure 6 Utilizing the PLSR, RF, and BPN methods along with optimal feature selection, the winter wheat yield is predicted in both the training set and the validation set

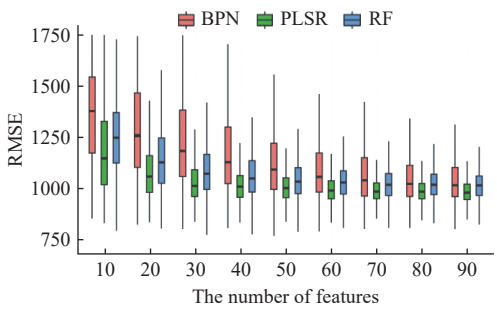

Figure 7 The performance variations of models with different sample sizes

Table 4 Performance variation table for models with different sample sizes

Model		The number of samples								
		10	20	30	40	50	60	70	80	90
PLSR	RMSE	1362.635	1117.195	1041.489	1022.825	1011.759	1000.409	994.992	991.187	988.522
	CV	0.39	0.21	0.11	0.09	0.08	0.07	0.06	0.06	0.06
RF	RMSE	1267.485	1148.79	1092.162	1064.229	1048.487	1037.283	1025.359	1026.235	1020.745
	CV	0.16	0.14	0.13	0.11	0.10	0.09	0.08	0.08	0.07
BPN	RMSE	2137.365	2084.072	2435.194	1250.637	1842.271	1136.04	1107.028	1090.82	1073.78
	CV	4.42	7.33	12.05	0.27	8.58	0.21	0.20	0.20	0.18

Note: CV represents the coefficient of variation.

3.4 Winter wheat yield mapping based on UAV

Figures 8 and 9 present UAV maps of winter wheat yield predictions for the years 2014-2015 and 2017-2018, respectively, providing a visual representation of regional yield variations. Further comparison of the UAV yield maps for the two years with fertilization levels revealed an increase in average yield with higher fertilizer application. Plots subjected to the N1 fertilization treatment exhibited the lowest average yield (3317.69 kg/hm^2), while those under the N4 fertilization treatment showed the highest average yield (9746.89 kg/hm^2). The consistency between predicted yields and fertilization patterns further emphasizes the reliability of yield prediction in this study.

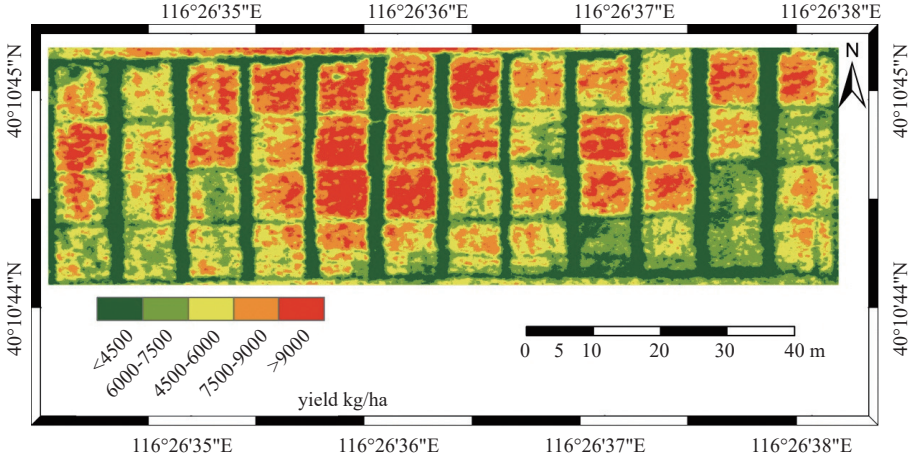

Figure 8 Yield maps of winter wheat based on the PLSR method and UAV hyperspectral imagery from 2014-2015

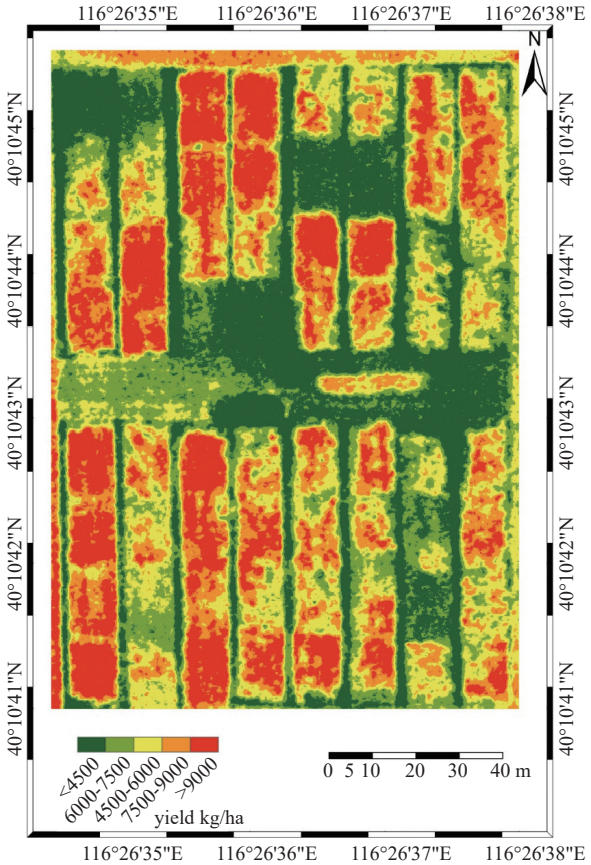

Figure 9 Yield maps of winter wheat based on the PLSR method and UAV hyperspectral imagery from 2017-2018

4 Discussion

In terms of crop production, VI can partially reflect plant growth. In this study, the correlation between VI and yield was compared, and the results revealed that the bands highly correlated with yield were concentrated in the infrared and near-infrared bands. Among them, NDRE (720 and 790 nm bands) had the highest correlation with yield. Juliane also pointed out that the near-infrared band is used to predict crop biomass with high accuracy[51]. Most traditional statistical analysis methods are based on a single VI, but the information contained in a single VI tends to be saturated[52]. In our study, multiple RS VI combinations can achieve information complementarity, compensate for the defects of the single VI, and improve the accuracy of RS yield prediction.

The appropriate selection of RS feature parameters can improve the accuracy of winter wheat RS prediction. However, when more parameters of RS features are selected, the accuracy of RS prediction is not necessarily good, and the RS characteristics highly correlated with winter wheat yield should be selected[53]. After the results shown in Figure 5 were compared, the accuracy of the yield prediction model based on PLSR and BPN did not improve with the increase in VI, whereas the accuracy of the yield prediction models based on RF improved with the increase in VI. Both PLSR and BPN algorithms require inputting feature parameters as sample sets, so complex collinear relations exist among many feature parameters, and the increased feature parameters cause information superposition and noise increase; thus, the accuracy of prediction models is affected[54]. The RF algorithm has a good tolerance to outliers and noise and is not easy to overfit[55]. Breiman studied the

relationship between a random feature number and RF intensity and the relationship between a random feature number and a generalization error[45]. Breiman found that RF intensity increases as random feature numbers increase, whereas the generalized error rate decreases slightly as random feature numbers increase[45]. Therefore, different VI models were built in this study, and the best VI was chosen to construct a yield prediction model and eliminate the influence of overfitting on the accuracy of the model.

The accuracy of the yield prediction model is affected by two factors: the inherent properties of crops and the number of samples and prediction methods[56]. Among them, different conclusions exist in different studies on the selection criteria of samples[57]. When the number of samples increases from 10 to 70 (Table 4), the prediction accuracy of models significantly improves. However, when the number of samples gradually increases from 70 to 90, the accuracy of the model does not improve significantly. This result indicated that at least 70 sample points were needed on the sample scale of this study, and the predicted results were credible. The performance of the RF model depends on the classification accuracy and diversity of each decision tree[58]. The weights and thresholds of BPN are random during each initialization, and the errors at the end of training are different[59]. As such, the results after each training are slightly different when RF and BPN models are used. The random results of RF and BPN production prediction models were analyzed, and the results revealed that the average value of the model results ($RMSE_{RF}$=1021.221 kg/hm^2, $RMSE_{BPN}$= 1069.863 kg/hm^2) was closer to the average value of the overall results when the random times of RF and BPN production prediction models reach 400 times.

Based on hyperspectral imagery obtained from UAV, prediction models were established using PLSR, RF, and BPN. The results of the PLSR yield prediction model outperformed the other models, providing support for accurate wheat yield prediction. As agricultural RS technology rapidly advances, an increasing number of yield prediction models are being developed. Further research will assess the adaptability of these models to different features and samples. In addition to VI features, attention should be given to texture features or features derived from spectral or spatial dimensions through other transformations[21]. This study conducted preliminary investigations into PLSR, RF, and BPN prediction models for winter wheat yield prediction using UAV hyperspectral RS. Future research may consider different wheat climates and planting conditions[16], evaluating the regional transferability of prediction models.

5 Conclusions

In this study, three models of PLSR, RF, and BPN for yield prediction in winter wheat were compared based on VIs from UAV-based hyperspectral reflectance data. This study demonstrates the optimal performance of the PLSR model in predicting wheat yield, showcasing remarkable stability and accuracy with an RMSE of 948.88 kg/hm^2. Contrary to the conventional notion that an increase in input features leads to heightened accuracy, our investigation reveals that the PLSR, RF, and BPN models exhibit peak performance when trained with the top 3, 8, and 4 VIs, respectively, exhibiting the highest correlation. Additionally, the study indicates that as the number of training samples rises, there is an observable enhancement in model accuracy, reaching a point of stability when the training samples reach 70. Employing PLSR and optimal feature scales, the generation of UAV yield prediction maps proves to be successful, offering crucial data support for field management, health monitoring, and precision decision-making.

Acknowledgements

This work was financially supported by the National Natural Science Foundation of China (Grant No. 42271396) and the Key R&D project of Hebei Province (Grant No. 22326406D).

[References]

[1] Devereux S. Livelihood insecurity and social protection: A re‐emerging issue in rural development. Development Policy Review, 2002; 19(4): 507–519.

[2] Gilmour B W. Achieving food security in China: The challenges ahead. China Agricultural Economic Review, 2019; 11(2): 443–446.

[3] Becker-Reshef I, Vermote E, Lindeman M, Justice C. A generalized regression-based model for forecasting winter wheat yields in Kansas and Ukraine using MODIS data. Remote Sensing of Environment, 2010; 114(6): 1312–1323.

[4] Leroux L, Castets M, Baron C, Escorihuela M-J, Bégué A, Lo Seen D. Maize yield estimation in West Africa from crop process-induced combinations of multi-domain remote sensing indices. European Journal of Agronomy, 2019; 108: 11–26.

[5] Liu H Y, Zhu H C. Hyperspectral characteristic analysis for leaf nitrogen content in different growth stages of winter wheat. Applied Optics, 2016; 55(34): D151–D161.

[6] Cho M A, Skidmore A K. A new technique for extracting the red edge position from hyperspectral data: The linear extrapolation method. Remote Sensing of Environment, 2006; 101: 181–193.

[7] Zhu H C, Liu H Y, Xu Y X, Y G J. UAV-based hyperspectral analysis and spectral indices constructing for quantitatively monitoring leaf nitrogen content of winter wheat. Applied Optics, 2018; 57(27): 7722–7732.

[8] McLellan E L, Cassman K G, Eagle A J, Woodbury P B, Sela S, Tonitto C, et al. The nitrogen balancing act: Tracking the environmental performance of food production. BioScience, 2018; 68(3): 194–203.

[9] Hama A, Tanaka K, Mochizuki A, Tsuruoka Y, Kondoh A. Estimating the protein concentration in rice grain using UAV imagery together with agroclimatic data. Agronomy, 2020; 10(3): 431.

[10] Jewan S Y Y, Pagay V, Billa L, Tyerman S D, Gautam D, Sparkes D, et al. The feasibility of using a low-cost near-infrared, sensitive, consumer-grade digital camera mounted on a commercial UAV to assess Bambara groundnut yield. International Journal of Remote Sensing, 2022; 43: 393–423.

[11] Yang G J, Liu J G, Zhao C J, Li Z H, Huang Y B, Yu H Y, et al. Unmanned aerial vehicle remote sensing for field-based crop phenotyping: current status and perspectives. Front. Plant Sci., 2017; 8: 1111.

[12] Wan L, Cen H Y, Zhu J P, Zhang J F, Zhu Y M, Sun D W, et al. Grain yield prediction of rice using multi-temporal UAV-based RGB and multispectral images and model transfer - a case study of small farmlands in the South of China. Agricultural and Forest Meteorology, 2020; 291: 108096.

[13] García-Martínez H, Flores-Magdaleno H, Ascencio-Hernández R, Khalil-Gardezi A, Tijerina-Chávez L, Mancilla-Villa O R, et al. Corn grain yield estimation from vegetation indices, canopy cover, plant density, and a neural network using multispectral and RGB images acquired with unmanned aerial vehicles. Agriculture, 2020; 10(7): 277.

[14] Wei L L, Yang H S, Niu Y X, Zhang Y N, Xu L Z, Chai X Y. Wheat biomass, yield, and straw-grain ratio estimation from multi-temporal UAV-based RGB and multispectral images. Biosystems Engineering, 2023; 234: 187–205.

[15] Xu X B, Nie C W, Jin X L, Li Z H, Zhu H C, Xu H G, et al. A comprehensive yield evaluation indicator based on an improved fuzzy comprehensive evaluation method and hyperspectral data. Field Crops Research, 2021; 270: 108204.

[16] Li Z H, Taylor J, Yang H, Casa R, Jin X L, Li Z H, et al. A hierarchical interannual wheat yield and grain protein prediction model using spectral vegetative indices and meteorological data. Field Crops Research, 2020; 248: 107711.

[17] Fan J H, Zhou J, Wang B W, de Leon N, Kaeppler S M, Lima D C, et al. Estimation of maize yield and flowering time using multi-temporal UAV-based hyperspectral data. Remote Sensing, 2022; 14(13): 3052.

[18] Kanning M, Kühling I, Trautz D, Jarmer T. High-resolution UAV-based

hyperspectral imagery for LAI and chlorophyll estimations from wheat for yield prediction. Remote Sensing, 2018; 10(12): 2000.
[19] Verrelst J, Rivera J P, Gitelson A, Delegido J, Moreno J, Camps-Valls G. Spectral band selection for vegetation properties retrieval using Gaussian processes regression. International Journal of Applied Earth Observation and Geoinformation, 2016; 52: 554–567.
[20] Wei H E, Grafton M, Bretherton M, Irwin M, Sandoval E. Evaluation of the use of UAV-derived vegetation indices and environmental variables for grapevine water status monitoring based on machine learning algorithms and SHAP analysis. Remote Sensing, 2022; 14(23): 5918.
[21] Zhou L L, Nie C W, Su T, Xu X B, Song Y, Yin D M, et al. Evaluating the canopy chlorophyll density of maize at the whole growth stage based on multi-scale UAV image feature fusion and machine learning methods. Agriculture, 2023; 13(4): 895.
[22] Muñoz J D, Finley A O, Gehl R, Kravchenko S. Nonlinear hierarchical models for predicting cover crop biomass using Normalized Difference Vegetation Index. Remote Sensing of Environment, 2010; 114(12): 2833–2840.
[23] Xu X B, He W, Zhang H Y. A novel habitat adaptability evaluation indicator (HAEI) for predicting yield of county-level winter wheat in China base on multisource climate data from 2001 to 2020. International Journal of Applied Earth Observation and Geoinformation, 2023; 125: 103603.
[24] Xu X B, He W, Zhang H Y. Random hierarchical model for estimation of wheat yield in the North China Plain at different spatial scales. Field Crops Research, 2024; 306: 109226.
[25] van Klompenburg T, Kassahun A, Catal C. Crop yield prediction using machine learning: A systematic literature review. Computers and Electronics in Agriculture, 2020; 177: 105709.
[26] Guo Y H, Fu Y S, Hao F H, Zhang X, Wu W X, Jin X L, et al. Integrated phenology and climate in rice yields prediction using machine learning methods. Ecological Indicators, 2021; 120: 106935.
[27] Tan C W, Luo M, Yang X, Ma C, Zhou J, Du Y, et al. Remote sensing estimation of wheat practical yield on regional scale using partial least squares regression algorithm based on HJ-1A/1B images. Transactions of the CSAE, 2015; 31(15): 161–166. (in Chinese)
[28] Su B, Liu L, Yang F T. Comparison and research of grain production forecasting with methods of GM(1, N) gray system and BPNN. Journal of China Agricultural University, 2006; 4: 99–104. (in Chinese)
[29] Yue J B, Yang G J, Feng H K. Comparative of remote sensing estimation models of winter wheat biomass based on random forest algorithm. Transactions of the CSAE, 2016; 32(18): 175–182.
[30] Holzman M E, Rivas R, Piccolo M C. Estimating soil moisture and the relationship with crop yield using surface temperature and vegetation index. International Journal of Applied Earth Observation and Geoinformation, 2014; 28: 181–192.
[31] Bolton D K, Friedl M A. Forecasting crop yield using remotely sensed vegetation indices and crop phenology metrics. Agricultural and Forest Meteorology, 2013; 173: 74–84.
[32] Ho T K. Random decision forests. In: Proceedings of the Proceedings of 3rd international conference on document analysis and recognition, 1995; pp.278–282.
[33] Li L C, Wang B, Feng P Y, Wang H H, He Q S, Wang Y K, et al. Crop yield forecasting and associated optimum lead time analysis based on multi-source environmental data across China. Agricultural and Forest Meteorology, 2021; 308–309: 108558.
[34] Turner D, Lucieer A, Wallace L. Direct georeferencing of ultrahigh-resolution UAV imagery. IEEE Transactions on Geoscience and Remote Sensing, 2014; 52(5): 2738–2745.
[35] Gitelson A A, Viña A, Ciganda V, Rundquist D C, Arkebauer T J. Remote estimation of canopy chlorophyll content in crops. Geophysical Research Letters, 2005; 32(8): 2005GL022688.
[36] Chen P F, Haboudane D, Tremblay N, Wang J H, Vigneault P, Li B G. New spectral indicator assessing the efficiency of crop nitrogen treatment in corn and wheat. Remote Sensing of Environment, 2010; 114(9): 1987–1997.
[37] Zarco-Tejada P J, Hornero A, Hernandez-Clemente R, Beck P S A. Understanding the temporal dimension of the red-edge spectral region for forest decline detection using high-resolution hyperspectral and Sentinel-2a imagery. ISPRS Journal of Photogrammety and Remote Sensing, 2018; 137: 134–148.
[38] Baret F, Guyot G. Potentials and limits of vegetation indices for LAI and APAR assessment. Remote Sensing of Environment, 1991; 35(2-3): 161–173.
[39] Chen J M. Evaluation of vegetation indices and a modified simple ratio for boreal applications. Canadian Journal of Remote Sensing, 2014; 22(3): 229–242.
[40] Sims D A, Gamon J A. Relationships between leaf pigment content and spectral reflectance across a wide range of species, leaf structures and developmental stages. Remote Sensing of Environment, 2002; 81(2-3): 337–354.
[41] Fitzgerald G, Rodriguez D, O'Leary G. Measuring and predicting canopy nitrogen nutrition in wheat using a spectral index - The canopy chlorophyll content index (CCCI). Field Crops Research, 2010; 116(3): 318–324.
[42] Bouman B A M. Linking physical remote sensing models with crop growth simulation models, applied for sugar beet. International Journal of Remote Sensing, 2007; 13(14): 2565–2581.
[43] Steddom K, Heidel G, Jones D, Rush C M. Remote detection of rhizomania in sugar beets. Phytopathology, 2003; 93(6): 720–726,
[44] Verrelst J, Schaepman M E, Koetz B, Kneubühler M. Angular sensitivity analysis of vegetation indices derived from CHRIS/PROBA data. Remote Sensing of Environment, 2008; 112(5): 2341–2353.
[45] Helland I S. On the structure of partial least squares regression. Communications in Statistics - Simulation and Computation, 1988; 17(2): 581–607.
[46] Breiman L. Random forests. Machine Learning, 2001; 45: 5–32,
[47] Genuer R, Poggi J-M, Tuleau-Malot C. Variable selection using random forests. Pattern Recognition Letters, 2010; 31(14): 2225–2236.
[48] Gao D, Zhang Y-X, Zhao Y-H. Random forest algorithm for classification of multiwavelength data. Research in Astronomy and Astrophysics, 2009; 9(2): 220–226,
[49] Liu H Y, Zhu H C, Wang P. Quantitative modelling for leaf nitrogen content of winter wheat using UAV-based hyperspectral data. International Journal of Remote Sensing, 2017; 38(8-10): 2117–2134.
[50] Li Z, Nie C, Wei C, Xu X, Song X, Wang J. Comparison of four chemometric techniques for estimating leaf nitrogen concentrations in winter wheat (*Triticum aestivum*) based on hyperspectral features. Journal of Applied Spectroscopy, 2016; 83: 240–247.
[51] Bendig J, Bolten A, Bennertz S, Broscheit J, Eichfuss S, Bareth G. Estimating biomass of barley using crop surface models (CSMs) derived from UAV-based RGB imaging. Remote Sensing, 2014; 6(1): 10395–10412.
[52] Son N T, Chen C F, Chen C R, Chang L Y, Duc H N, Nguyen L D. Prediction of rice crop yield using MODIS EVI−LAI data in the Mekong Delta, Vietnam. International Journal of Remote Sensing, 2013; 34(20): 7275–7292.
[53] Qader S H, Dash J, Atkinson P M. Forecasting wheat and barley crop production in arid and semi-arid regions using remotely sensed primary productivity and crop phenology: A case study in Iraq. Science of the Total Environment, 2018; 613-614: 250–262.
[54] Yang F Q, Dai H Y, Feng H K, Yang G J, Li Z H, Chen Z X. Hyperspectral estimation of plant nitrogen content based on Akaike's information criterion. Transactions of the CSAE, 2016; 32(23): 161–167. (in Chinese)
[55] Zhou Q F, Zhou H, Li T. Cost-sensitive feature selection using random forest: Selecting low-cost subsets of informative features. Knowledge-Based Systems, 2016; 95: 1–11.
[56] Liu H L, Yang J Y, He P, Bai Y L, Jin J Y, Drury C F, et al. Optimizing parameters of CSM-CERES-maize model to improve simulation performance of maize growth and nitrogen uptake in Northeast China. Journal of Integrative Agriculture, 2012; 11(11): 1898–1913.
[57] Chai X R, Huang Y F. Comparison of spatial prediction of soil properties under different sampling sizes. Scientia Agricultura Sinica, 2013; 46(22): 4716–4725. (in Chinese)
[58] Malekipirbazari M, Aksakalli V. Risk assessment in social lending via random forests. Expert Systems with Applications, 2015; 42(10): 4621–4631.
[59] Qu Y, Wang M, Dong W X, Wang Y H. Prediction of atmospheric ammonia concentration in farmlands using BP neural network. Chinese Journal of Eco-Agriculture, 2019; 27(4): 519–528. (in Chinese)